DOI 10.1007/s10812-023-01647-y
Journal of Applied Spectroscopy, Vol. 90, No. 5, November, 2023 (Russian Original Vol. 90, No. 5, September–October, 2023)

FABRICATION AND CHARACTERIZATION OF NANOCRYSTALLINE LEAD SULFIDE THIN FILM FOR VISIBLE LIGHT PHOTODETECTOR

Sandip V. Bhatt, Rakesh V. Patel,* Sefali R. Patel, Krishna Joshi, Akshay Jadav, Monank Patel, Dhruv Desai, and S. H. Chaki

UDC 535.34;539.216.2

This study focuses on the preparation of a high-performance visible light photodetector using nanocrystalline lead sulphide (PbS) thin films. The thin films were deposited onto glass substrates via the chemical bath deposition technique, utilizing an aqueous solution of lead acetate and thiourea. The structural study carried out on the deposited films by X-ray diffraction exhibited a cubic crystal structure with a PbS phase. The optical characteristics of PbS thin films were investigated employing UV-Vis absorption spectroscopy. The absorption spectroscopy was carried out in the wavelength range of 400–1000 nm. The absorbance spectra were utilized to calculate the spectral dependence of several optical parameters: band gap, refractive index, extinction coefficient, dielectric constant, and optical and electrical conductivity. The photocurrent was measured in nanocrystalline PbS thin films under the illumination of specific LED wavelength sources. The quality of the PbS thin film as a photodetector was investigated by determining the rise time, decay time, photosensitivity, specific detectivity, and external quantum efficiency.

Keywords: *PbS thin film, X-ray diffraction, UV-Vis absorption spectroscopy, photodetector.*

Introduction. A photodetector, also known as a photosensor, has recently emerged as a potential optoelectronic device for various applications such as surveillance systems in night vision, military missile tracking, deep tissue imaging, industry defect imaging, environmental sensing, and astronomy [1, 2]. Depending on the band gap of semiconducting materials, a photodetector is able to detect ultraviolet, visible, and infrared regions of the electromagnetic spectrum. In the current scenario, nanostructure semiconducting materials are in demand for modern photonics and are capable of detecting a broad spectrum as a photodetector. Commercial photodetectors are typically fabricated using semiconducting materials consisting of silicon/germanium, A^{II}–B^{VI}/A^{III}–B^{V} group semiconductor alloys, A^{IV}–B^{VI} group (SnS, PbSe), gallium phosphide (GaP) and silicon carbide (SiC) material systems [3, 4]. Among these, the IV–VI group semiconductors have recently gained much attention and have found many applications in various optoelectronic devices. One of the most attractive candidates of this group is lead sulphide (PbS), due to its numerous applications ranging from infrared technology [5], solar cell [6], infrared LED [7], diode lasers [8], humidity and temperature sensors [9] and electrochemical storage devices [10]. Lead sulphide (PbS) has a low effective mass of electrons (~0.1m_e), a high dielectric constant (17.2), and a relatively large exciton Bohr radius of 18 nm. Additionally, PbS exhibits extraordinary size-dependent properties at the nanoscale, which makes it possible to easily tune the band gap of this nanocrystalline semiconductor from 0.41 (bulk) to 4 eV by selecting the appropriate particle size [11]. Consequently, PbS nanocrystallites exhibit some novel electrical and optical properties, including a blue shift of the optical absorption, size-dependent luminescence, and exceptional third-order nonlinear effect [12]. The aforementioned properties make PbS a feasible material for the high absorption of solar spectra.

Several fabrication techniques, including spin coating [13], spray pyrolysis [14], electrodeposition [15], pulsed laser deposition [16], and chemical bath deposition (CBD) [17], have been utilized in recent years to deposit PbS thin films for photodetector applications. Among these methods, the CBD stands out as the most cost-effective, scalable and simple technique. CBD also does not require high-end instrumentation and is easy to control for depositions [18].

The PbS has been used as an IR detector by various research groups all over the world [5, 18], but there are very few studies on its use as a visible light detector. Vankhade et al. [19] investigated the photoconductivity of PbS nanocrystalline

*To whom correspondence should be addressed.

Department of Applied and Interdisciplinary Sciences (CISST), Sardar Patel University, Vallabh Vidyanagar, Gujarat, India; email: drrvpatel@gmail.com. Abstract of article is published in Zhurnal Prikladnoi Spektroskopii, Vol. 90, No. 5, p. 813, September–October, 2023.

thin films with increasing thickness using a halogen lamp. Devidas et al. [14] measured the photosensitivity of PbS film under 100 W tungsten lamp irradiation. Furthermore, Khanzode et al. [20, 21] reported a flexible paper-based photodetector study employing a nano-crystalline lead-sulfide thin film using a typical 100 W tungsten lamp as the light source. The photo *I–V* electrical measurement on PbS nanosheets with different light intensities of the tungsten lamp was examined by Shkir et al. [22]. Jungang He et al. [23] studied a photoconductive photodetector fabricated from PbS colloidal quantum dots that exhibited extremely high sensitivity and detectivity when exposed to 650 nm LED incident light. Conventionally, metal oxides (such as Sb_2O_3, V_2O_5, ZnO, CuO, and CdO), transition metal dichalcogenides (such as ReS_2, $MoSe_2$, and WS_2), and perovskites have been used to demonstrate visible-light photodetectors [24]. However, there are very limited papers published related to PbS thin film as a visible photodetector. Hence, it was the intention of the authors to study PbS as the sole photoconductive detector material for the entire Vis-NIR spectrum without the usage of any other semiconductor. The objective is to develop a low-cost, highly efficient visible light photodetector based on PbS nanocrystalline thin film. Here, the nanocrystalline PbS thin films were deposited using the chemical bath deposition (CBD) technique, and photoconductivity analysis is performed for wavelengths in the visible range.

Experimental. Nanocrystalline PbS thin films were deposited on precleaned glass substrates using the CBD technique at room temperature. The glass substrate was precleaned using acid, detergent, and distilled water washes followed by acetone, then dried in a hot air oven. A precursor solution consisting of lead acetate trihydrate ($(CH_3COO)_2Pb \cdot 3H_2O$) and thiourea ($CS(NH_2)_2$) was used as the Pb^{2+} and S^{2-} sources, respectively. The synthesis process involves the preparation of a mixed solution of lead acetate trihydrate (0.06 mol/L) and thiourea (0.3 mol/L) in 20 mL distilled water. The pH of the solution was adjusted to 10 by adding ammonium hydroxide drop by drop. The cleaned glass slides were then immersed vertically in the solution for 6 h without touching the beaker walls. During this period, the color of the solution changed to brownish-black, indicating the initiation of a chemical reaction. After the film deposition was completed, the slide was taken out of the solution and washed multiple times with distilled water, dried at room temperature, and used for further characterization. The thickness of the PbS thin films was determined using the gravimetric weight difference method with an electronic microbalance. The glass substrate was weighed before (w_1) and after the deposition (w_2), and the thickness of the films (t) was calculated using the formula $t = (w_2 - w_1)/\rho A$, where ρ is the density of the PbS material, and A is the area of the deposited film. It is observed that the thickness of the PbS nanocrystalline thin film lies in the range of ~ 400 ± 20 nm.

The X-ray diffraction (XRD) pattern of the films was obtained using a Righaku Ultima-IV X-ray diffractometer employing CuK_α radiation with operating conditions of 30 mA and 40 kV. The optical absorption spectrum was recorded using a Perkin Elmer Lambda-19 UV-Vis spectrophotometer. The PbS nanocrystalline thin film deposited on glass slides was cut to 1 × 1 cm^2 pieces and used for electrical measurements. Proper electrical contact was put on the surface of the PbS thin films using thin copper wire and conductive silver (Ag) paste by keeping the electrode gap of 10 mm. Keithley semiconductor characterization (Model-4200 SCS) was employed for current–voltage (*I–V*) measurements of the films. Photoconductivity measurements were carried out using a 10 W LED source with different wavelengths 450, 550, 580, and 650 nm at an intensity of 10 mW/cm^2 illumination.

Results and Discussions. *X-ray diffraction.* The XRD pattern of the as-deposited PbS thin films on the glass substrate is shown in Fig. 1. It exhibited four broad major peaks corresponding to (111), (200), (220), and (311). The XRD pattern also shows several low-intensity background noise peaks, arising due to the amorphous glass substrate. All observed diffracted peaks are in good agreement with that of the standard JCPDS data Card No. 05-0592, indicating that the films are pure cubic PbS with no other phase. The calculated value of the lattice parameter of the as-deposited PbS thin film is 5.93 Å, which matches the reported data [25]. The broadening in the peaks of the XRD patterns is mainly attributed to the crystallite size and micro-strain. The apparent crystallite size and micro-strain are estimated using Scherrer's formula using FWHM and peak position [26]:

$$D = \frac{k\lambda}{\beta \cos \theta}, \tag{1}$$

$$\varepsilon = \frac{\beta}{4 \tan \theta}, \tag{2}$$

where k is 0.9, considering the particles to be spherical in shape, λ is the X-ray wavelength of CuK_α radiation (1.5406 Å), β is the full width at half maximum (FWHM) in radians of the diffraction peaks, θ is the diffraction angle, and ε is the microstrain. The microstrain originates due to the presence of defects in the lattice, such as vacancies, grain boundaries, etc.

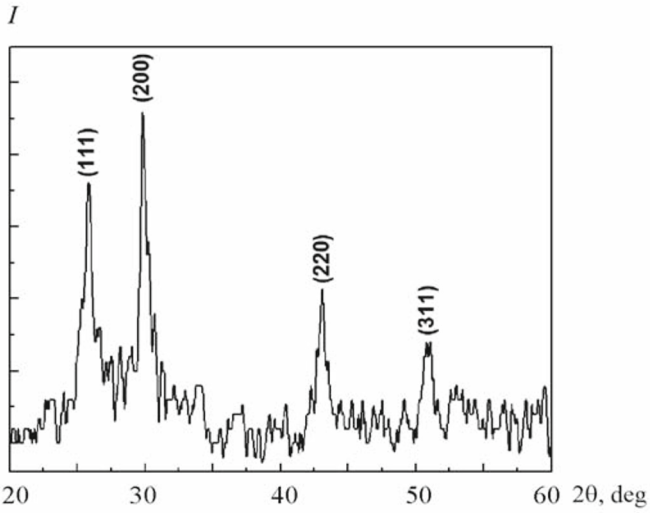

Fig. 1. The XRD pattern of as-deposited PbS thin films.

The average crystallite size came out to be ~18 nm, indicating that the PbS film is nanocrystalline in nature. The calculated microstrain value is 0.0039, whereby the positive value indicates that the strain is of tensile type. The approximate dislocation density is calculated using Williamson and Smallman's formula [27], $\delta = 1/D^2$, where D is the crystallite size. The estimated dislocation density for the deposited PbS thin films came to 3.08×10^{15} m^{-2}.

UV-Vis spectroscopy. The absorbance spectrum of the as-deposited PbS thin films in the wavelength range of 400 nm to 1000 nm is shown in the inset of Fig. 2. The absorbance shows a noticeable blue shift in the present PbS nanocrystalline thin film compared to the bulk PbS, which possesses an absorbance of around 3100 nm [12]. The blue shift suggests quantum confinement arising due to the nanocrystallite size effect. The optical absorption coefficient (α) of the nanocrystalline PbS thin films is calculated using the equation $\alpha = 2.303A/t$, where A is the absorbance and t is the thickness of PbS thin film [28]. The optical absorption coefficients throughout the measured wavelength range are of the order of 10^7 m^{-1}. Higher values of α imply a higher probability of a direct transition between extended states in conduction and valence bands. The high optical absorption coefficient of the films in the visible wavelength region makes them suitable for visible light photodetector applications. The optical energy gap (E_g) of PbS thin films is calculated using the Tauc relation [29]:

$$(\alpha h\nu)^n = A(h\nu - E_g), \tag{3}$$

where α is the absorption coefficient, ν is the frequency of the incident photon, h is Planck's constant, A is the absorbance, E_g is the bandgap, and $n = 2$ corresponds to a direct allowed transition. Figure 2 shows the Tauc plot in which $(\alpha h\nu)^2$ is plotted against energy ($h\nu$), and the direct bandgap energy is calculated by extrapolating the straight region of the curve to zero absorption coefficients. The obtained optical bandgap of the as-deposited PbS thin film is 2.08 eV. The obtained value is nearly 1.67 eV higher than the E_g of bulk PbS, which is 0.41 eV [12], indicating a blue shift. The blue shift in E_g is attributed to the nanocrystalline nature of the deposited PbS thin film.

The study of optical parameters such as extinction coefficient (k), refractive index (η), dielectric constant (ε), etc., of a material explains the phenomenon of light interaction with the material. The parameters are usually correlated to the atomic structure, electronic band structure, and electrical properties of the material. Therefore, investigating optical behaviour is critical to understanding the functionality of optoelectronic devices. Here the optical parameters of the synthesized PbS thin films are studied to understand the size effect on these parameters. The extinction coefficient (k) measures the fraction of light that gets scattered or absorbed over a unit distance when it passes through the medium. The quantity k is related to the optical absorption coefficient by the following equation [28]:

$$k = \frac{\alpha\lambda}{4\pi}. \tag{4}$$

Figure 3 shows the variation of k with wavelength for the PbS thin film. The plot shows an initial increase followed by a continuous decrease of k with increasing wavelength. At lower wavelengths, the higher value of k indicates light loss

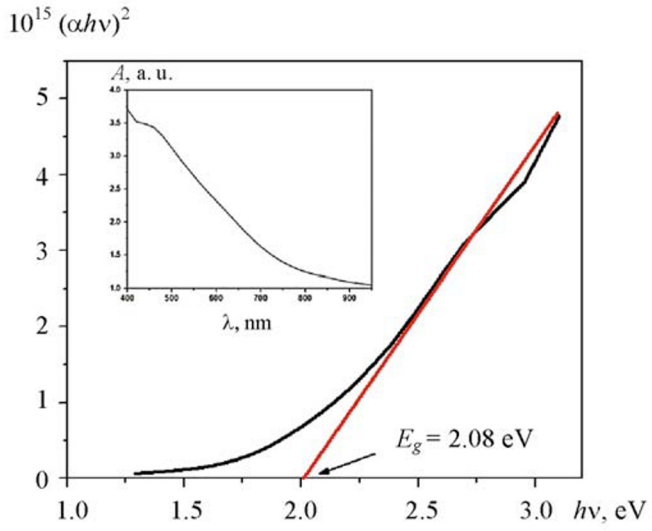

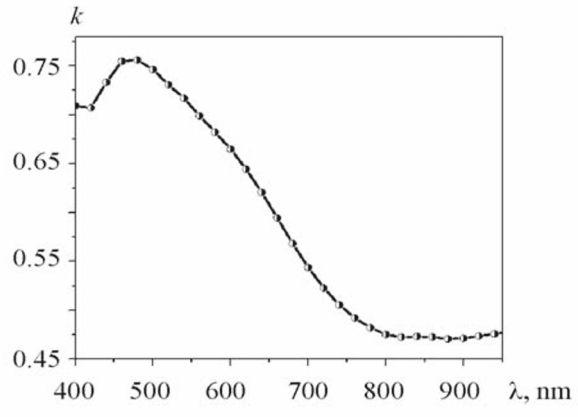

Fig. 2. The Tauc plot and absorbance spectrum (insight) of PbS thin film.

Fig. 3. The extinction coefficient (k) variation against wavelength.

due to scattering or absorption, whereas at higher wavelengths, the decrease in k indicates an increase in the transparency of the thin films. The low linear variation of k with a wavelength in the near-infrared regions indicates the PbS thin films have potential in optoelectronic applications.

The refractive index (η) of the prepared PbS thin films was calculated using Herve and Vandamme's formula as [28]:

$$\eta^2 = 1 + \left(\frac{A}{E_g + B} \right)^2 , \tag{5}$$

where A = 13.6 and B = 3.4 eV [28]. The calculated value of η for the PbS thin film came out to be 2.75.

The complex dielectric constant (ε) [30, 31] is related to the refractive index (η) and the extinction coefficient (k) by $\varepsilon = \eta + ik$. The dielectric constant (ε) is a combination of the real dielectric constant (ε_r) and the imaginary dielectric constant (ε_i) related as $\varepsilon = \varepsilon_r + \varepsilon_i$, where $\varepsilon_r = \eta^2 - k^2$ and $\varepsilon_i = 2\eta k$. The real part of the dielectric constant describes how rapidly the light slows down as it travels through the material, whereas the corresponding imaginary part describes the loss due to polarization in the medium. The plots of complex, real and imaginary parts of the dielectric constant for the nanocrystalline PbS thin film are shown in Fig. 4. The variation study shows that the complex and imaginary parts of the dielectric constant are minimum and stable in the near infra-red wavelength regions. The observation is in line with the behaviour of extinction coefficient (k) with wavelength, thus corroborating each other's results.

The optical conductivity (σ_o) value is calculated using the following [17]:

$$\sigma_o = \frac{\alpha \eta c}{4\pi} , \tag{6}$$

where c is the velocity of light in vacuum. The electrical conductivity (σ_e) is determined using the relation [30]:

$$\sigma_e = \frac{2\lambda\sigma_o}{\alpha} . \tag{7}$$

The variation of σ_o and σ_e with wavelength for PbS thin films is shown in Fig. 5. The variation shows that the optical conductivity (σ_o) decreases with an increase in wavelength, whereas the electrical conductivity (σ_e) increases with wavelength value.

Photoconductive I–V studies. The photoconductive study on PbS thin films was done by measuring typical current-voltage (I–V) characteristics. The I–V characteristics are measured in the applied bias range of –5 to +5 V. The measurement

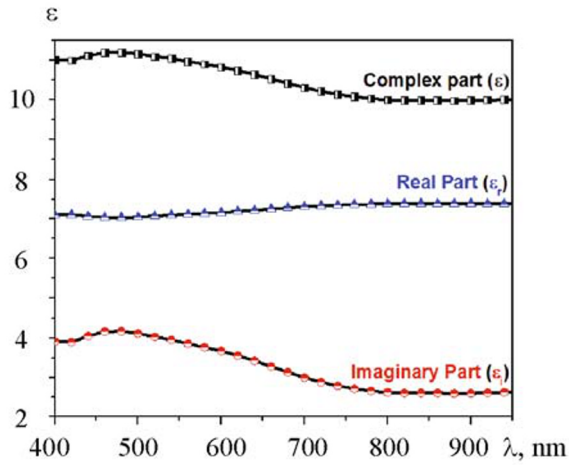

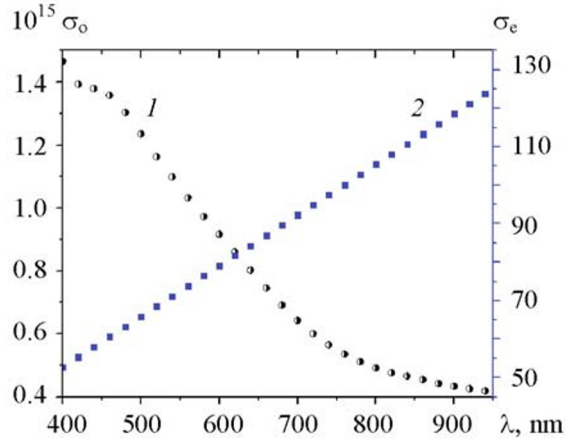

Fig. 4. The dielectric constant (ε) variation with wavelength of PbS thin film.

Fig. 5. Optical conductivity σ_o (1) and electrical conductivity σ_e (2) as a function of wavelength for PbS thin film.

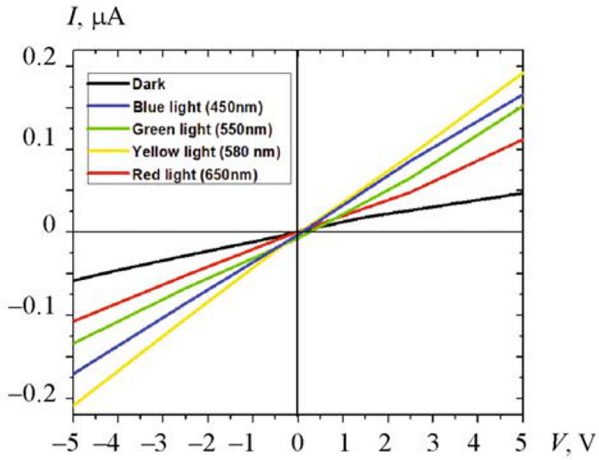

Fig. 6. Dark and illuminated *I–V* characteristic of PbS thin film as photodetector.

is carried out for both dark and illuminated conditions. The illumination study is done using LED sources of different wavelengths. The different wavelength of light used for the study are 450, 550, 580, and 650 nm. The *I–V* characteristics of nanocrystalline PbS films for both dark and illuminated conditions are shown in Fig. 6. All the *I–V* plots are straight lines passing through the origin, indicating that the contacts are perfect ohmic. The *I–V* characteristics for different wavelengths show an increase in current values with illumination, indicating that the thin films are photosensitive. The increase in current with illuminations is caused by the strong interaction of light with the PbS structure leading to the breaking of covalent bonds via photo-excitation in turn leading to a generation of free charge carriers [31]. This photo-generated charge carrier enhances the current with illumination.

The maximum dark current value observed at +5 V is approximately 47 nA, and the maximum current observed for the yellow incident wavelength (580 nm) is around 200 nA. The utmost photoresponse for the incident yellow wavelength is due to the matching of the bandgap of PbS (2.08 eV) with that of the energy of the yellow wavelength (~2.13 eV).

The photocurrent (I_{ph}) is calculated by taking the difference between the illuminated current and the dark current [32]; $I_{ph} = I_{ill} - I_{dark}$. Here, I_{ph} is the photocurrent, I_{ill} is current under an illumination condition, and I_{dark} is the current in a dark condition. The calculated values of the photocurrent at a bias voltage of +5 V are shown in Table 1. The maximum I_{ph}

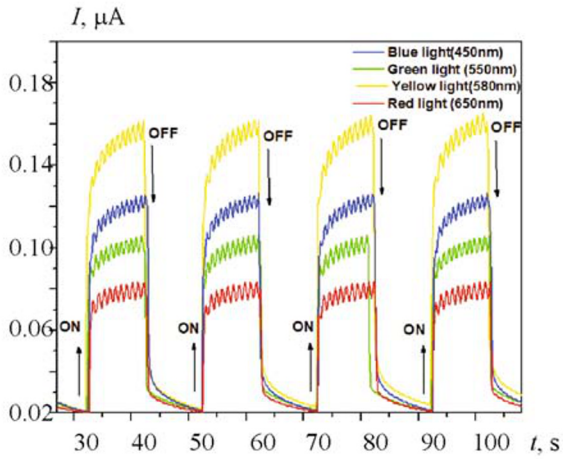

Fig. 7. Real-time-dependent photodetection measurement at an applied voltage of ±5 V.

is observed for yellow light. This maximum I_{ph} is attributed to the significant absorption of yellow light leading to maximum electron–hole pair generation.

The pulse photo-response experiment of an as-deposited PbS thin film photodetector is measured at a bias voltage of +5 V under continuous ON and OFF cycles for blue, green, yellow and red lights with a duration of 10 s each. The characteristics are shown in Fig. 7. The photocurrents increase sharply whenever the light is switched ON and decrease as the light is turned OFF. The magnitude of the photocurrent at each wavelength returns to the same level after each cycle without baseline shifting, thereby confirming that the detector is stable with good repeatability. When illuminated with blue light, the photocurrent increases quickly to a saturation value (~0.125 μA), while quickly falling to the dark current level (~0.02 μA) as the light is turned off. A similar rapid increase in the photocurrent is observed under green, yellow and red light illumination with a maximum current of ~0.105, 0.160, and ~0.083 μA, respectively. In the off condition, the photocurrent decreases exponentially over a short period of time to reach the dark current value.

An important parameter of any photodetector is its response time, which is defined as the interval of time required to increase the photocurrent from the dark current to the maximum photocurrent by 63%. The decay time is defined as the interval required to decrease the photocurrent from the maximum photocurrent to the dark current by 37%. The estimated rise time and decay time for different incident light wavelengths under a constant biasing voltage are tabulated in Table 1. Analysis of the data shows that the decay time is higher than the rise time, which is attributed to carriers getting trapped by surface defects or deep level defect states [33].

Other important parameters that affect the quality of a photodetector are its sensitivity, photoresponsivity, and specific detectivity. The sensitivity, photoresponsivity (R_λ), and specific detectivity (D) of the as-deposited PbS thin film are determined using the following equations [32, 33].

$$\text{Sensitivity (\%)} = (I_{ph}/I_{dark}) \times 100 \,, \tag{8}$$

$$R_\lambda = I_{ph} / P\Delta S \,, \tag{9}$$

$$D = \frac{R_\lambda S^{1/2}}{(2eI_{dark})^{1/2}} \,, \tag{10}$$

where P is the power intensity of incident light, S is the effective area of the photodetector (~1 cm^2), and e is the charge of an electron. The highest photosensitivity of 313% is observed for yellow light sources which is caused by matching of the yellow wavelength energy with the bandgap of PbS, leading to enhanced generation of electron–hole pairs.

The external quantum efficiency (EQE%) is another significant parameter used to characterize the photodetector. This parameter quantifies the amount of photogenerated charge carriers produced per incident photon. It is expressed as [34]:

$$\text{EQE\%} = \frac{R_\lambda hc}{e\lambda} \times 100 \,, \tag{11}$$

TABLE 1. Photocurrent, Rise Time and Decay Time of as Deposited PbS Thin Film at Different Wavelengths

Parameter	Light source wavelength, nm			
	450	550	580	650
Photocurrent, μA	0.123	0.105	0.145	0.065
Rise time, s	0.67	0.48	0.67	0.51
Decay time, s	1.12	1.13	1.13	1.13
Photosensitivity, %	259	221	306	138
Photoresponsivity, A/W	1.23×10^{-5}	1.05×10^{-5}	1.45×10^{-5}	0.65×10^{-5}
Specific detectivity, J	9.98×10^{6}	8.52×10^{-6}	1.18×10^{7}	5.27×10^{6}
EQE%	3.40×10^{-3}	2.37×10^{-3}	3.11×10^{-3}	1.24×10^{-3}

where h is Planck's constant, λ is the illumination wavelength, e is the electronic charge, c is the velocity of light, and R_λ is the photoresponsivity at a specific wavelength. Higher values of EQE indicate excellent sensitivity of the as-deposited PbS nanocrystalline thin films.

Conclusions. Nanocrystalline PbS thin films with a thickness of approximately 400 nm were successfully deposited using the chemical bath deposition technique. The XRD analysis revealed that the deposited thin films possess a cubic unit cell structure with a lattice parameter of 5.93 Å. The crystal structure and lattice parameters are in good agreement with the standard value. The average crystallite size was determined to be around 18 nm, with a micro-strain of a tensile type and a dislocation density of approximately 3.08×10^{15} m^{-2}. The absorbance study showed that the as-deposited PbS thin film has a direct optical bandgap of 2.08 eV. The variation of optical parameters with wavelengths indicated that the as-deposited PbS thin film has a stable response in the visible wavelength range. The *I–V* characteristics study for the as-deposited PbS thin film for dark and the four different incident wavelengths (dark, 450, 550, 580, and 650 nm) showed good photoresponse. The maximum photocurrent was observed for the 580 nm wavelength yellow light. The as-deposited PbS thin films exhibited good pulsed photoresponse to all four incident wavelengths. The determined photoresponse parameters suggest that the PbS thin films deposited through chemical bath deposition have potential for use as photodetectors.

Acknowledgement. The authors would like to express their gratitude to the DST Purse facility under CISST, Sardar Patel University for granting permission to use the Keithley semiconductor characterization instrument (Model-4200 SCS).

REFERENCES

1. C. L. Tan and H. Mohseni, *Nanophotonics*, **7**, 169–197 (2018); doi: 10.1515/nanoph-2017-0061.
2. P. Martyniuk, J. Antoszewski, M. Martyniuk, L. Faraone, and A. Rogalski, *Appl. Phys. Rev*., **1**, Article ID 041102 (2014); doi: 10.1063/1.4896193.
3. A. Rogalski, *Opto-Electron. Rev*., **20** (2012); doi: 10.2478/s11772-012-0037-7.
4. N. Gupta, J. Kedia, and A. Sharma, *Opt. Eng*., **60** (2021); doi: 10.1117/1.oe.60.9.090901.
5. E. Pentia, L. Pintilie, I. Matei, T. Botila, and I. Pintilie, *Infrared Phys. Tech.*, **44**, 207–211 (2003); doi: 10.1016/s1350-4495(02)00225-6.
6. C. Borriello, A. Bruno, R. Diana, T. Di Luccio, P. Morvillo, and R. Ricciardi, *Phys. Status Solidi* (*a*), **212**, 245–251 (2014); doi: 10.1002/pssa.201400213.
7. M. Kim and B. Park, *Appl. Sci*., **10**, 7440 (2020); doi:10.3390/app10217440.
8. L. Yun, Y. Qiu, C. Yang, J. Xing, K. Yu, and X. Xu, *Photon. Res*., **6**, 1028 (2018); doi: 10.1364/prj.6.001028.
9. X. Chen, J. Hu, P. Chen, M. Yin, F. Meng, and Y. Zhang, *Sens. Act. B: Chem*., **339**, Article ID 129902 (2021); doi: 10.1016/j.snb.2021.129902.
10. L. S. Chongad, A. Sharma, M. Banerjee, and A. Jain, *J. Phys.: Conf. Ser*., **755**, 012032 (2016); doi: 10.1088/1742-6596/755/1/012032.
11. D. Vankhade and T. K. Chaudhuri, *AIP Conf. Proc*. (**2018**); doi: 10.1063/1.5028771.
12. S. V. Bhatt, M. P. Deshpande, B. H. Soni, N. Garg, and S. H. Chaki, *Solid State Phenom*., **209**, 111–115 (2013); doi: 10.4028/www.scientific.net/ssp.209.111.

13. J. Patel, F. Mighri, A. Ajji, D. Tiwari, and T. K. Chaudhuri, *Appl. Phys. A*, **117**, 1791–1799 (2014); doi:10.1007/s00339-014-8659-x.
14. D. I. Halge, V. N. Narwade, P. M. Khanzode, J. W. Dadge, A. S. Rana, and K. A. Bogle, *AIP Conf. Proc.* (**2020**); doi: 10.1063/5.0001670.
15. I. Lucky, E. Simon, and I. Okeoghene, *Asian J. Chem. Sci*., **3**, 1–8 (2018); doi: 10.9734/ajocs/2017/40415.
16. T. V. Beatriceveena, E. Prabhu, V. Jayaraman, K. I. Gnanasekar, *Mater. Lett*., **238**, 324–327 (2019); doi: 10.1016/j.matlet.2018.12.038.
17. M. M. Abbas, A. A.-M. Shehab, A.-K. Al-Samuraee, and N.-A. Hassan, *Energy Proc*., **6**, 241–250 (2011); doi: 10.1016/j.egypro.2011.05.028.
18. A. B. Rohom, P. U. Londhe, P. R. Jadhav, G. R. Bhand, and N. B. Chaure, *J. Mater. Sci.: Mater. Electron*., **28**, 17107–17113 (2017); doi: 10.1007/s10854-017-7637-4.
19. D. Vankhade, A. Kothari, and T. K. Chaudhuri, *J. Electron. Mater*., **45**, 2789–2795 (2016); doi: 10.1007/s11664-016-4364-1.
20. P. M. Khanzode, D. I. Halge, V. N. Narwade, K. D. More, S. Begum, S. Taha, et al., *Int. Conf. Multifunctional Materials (ICMM-2019)* (2020); doi: 10.1063/5.0019617.
21. P. M. Khanzode, D. I. Halge, V. N. Narwade, J. W. Dadge, K. A. Bogle, *Optik*, **226**, 165933 (2021); doi: 10.1016/j.ijleo.2020.165933.
22. M. Shkir, I. M. Ashraf, and S. AlFaify, *Phys. Scr*., **94**, Article ID 025801 (2019); doi: 10.1088/1402-4896/aaf55a.
23. J. He, M. Luo, L. Hu, Y. Zhou, S. Jiang, H. Song, et al., *J. Alloys Compd*., **596**, 73–78 (2014); doi: 10.1016/j.jallcom.2014.01.194.
24. H.-J. Song, M.-H. Seo, K.-W. Choi, M.-S. Jo, J.-Y. Yoo, and J.-B. Yoon, *Sci. Rep*., **9** (2019); doi: 10.1038/s41598-019-43667-9.
25. S. V. Bhatt, M. P. Deshpande, S. H. Chaki, N. H. Patel, N. Pandy, B. H. Soni, et al., *AIP Conf. Proc*. (**2011**); doi:10.1063/1.3605844.
26. B. H. Soni, M. P. Deshpande, S. V. Bhatt, S. H. Chaki, and V. Sathe, *J. Appl. Spectr*., **79**, 901–907 (2013); doi: 10.1007/s10812-013-9692-9.
27. P. Rajput, M. P. Deshpande, H. R. Bhoi, N. M. Suchak, P. H. Desai, S. H. Chaki, et al., *Chem. Phys. Impact*, **5**, Article ID 100101 (2022); doi: 10.1016/j.chphi.2022.100101.
28. B. Sharma, R. Lalwani, and R. Das, *J. Mater. Sci.: Mater. Electron*., **33**, 11601–11612 (2022); doi: 10.1007/s10854-022-08132-w.
29. B. H. Soni, M. P. Deshpande, S. V. Bhatt, N. Garg, N. N. Pandya, and S. H. Chaki, *J. Optics*, **42**, 328–334 (2013); doi: 10.1007/s12596-013-0136-y.
30. S. Rajathi, K. Kirubavathi, and K. Selvaraju, *Arab. J. Chem*., **10**, 1167–1174 (2017); doi: 10.1016/j.arabjc.2014.11.057.
31. K. Paulraj, S. Ramaswamy, I. S. Yahia, A. M. Alshehri, H. H. Somaily, and H.-S. Kim, *Appl. Phys. A*, **126** (2020); doi: 10.1007/s00339-020-03686-0.
32. B. G. Valmik, M. P. Deshpande, S. V. Bhatt, V. Sathe, H. R. Bhoi, P. Rajput, et al., *Phys. B: Cond. Matter*., **614**, Article ID 413027 (2021); doi: 10.1016/j.physb.2021.413027.
33. H. Zhang, W. Wang, S. P. Yip, D. Li, F. Li, C. Lan, et al., *J. Mater. Chem. C*, **8**, 17025–17033 (2020); doi: 10.1039/d0tc04330c.
34. J. M. Wu and W. E. Chang, *ACS Appl. Mater. AMP, Interfaces*, **6**, 14286–14292 (2014); doi: 10.1021/am503598g.